Roughness replication in neutron supermirrors and periodic multilayers

T. Veres, L. Cser, Sz. Bálint and Sz. Sajti

Institutions

ABSTRACT

Interface roughness strongly influences the reflectivity of neutron supermirrors (SM) the major components of neutron optical devices. The in-plane and out-of-plane correlation of the interface roughness was studied using neutron and X-ray off-specular reflectometry in DC-sputtered Ni-Ti SMs and periodic multilayers. Roughness correlation is manifested in diffuse scatter plateaus and peaks which are interpreted in terms of Resonant Diffuse Scattering (RDS). A lower estimate of a few 1000 Å out-of-plane correlation length was found by off-set X-ray diffuse scans for periodic Ni-Ti multilayers of various bilayer thicknesses. Detector scans were carried out to observe off-specular neutron scattering from normal and reverse layer sequence SMs. The first order RDS is absent in normal but present in reverse sequence SMs, which is qualitatively explained by kinematical considerations. Distorted Wave Born Approximation simulations of off-specular scattering pattern both of normal and reverse SMs quantitatively reproduces the characteristic features of the measured curves with reasonable parameters, i.e. in-plane and out-of-plane correlation lengths and Hurst parameter of 1200 Å, 4000 Å, 7 Å and 0.5, respectively. The out-of-plane correlation length estimations deduced from SM and periodic multilayer reflectivities are in reasonable agreement with each other.

1. Introduction

Supermirror (SM) neutron guides have become a standard solution for transporting, shaping, bending and focusing neutron and x-ray beams. A SM is a depth-graded d-spacing multilayer, in which the layer thickness of each layer is designed as to ensure high reflectivity of the mirror over a broad angular / wavelength range of neutron or x-or VUV-rays. Neutron super-mirrors were invented in 1970s by Mezei (Mezei, 1976), (Mezei & Dagleish, 1977). The nowadays most widespread algorithm for SM design was developed by Hayter and Mook (1989). The performance of the SMs depends on the roughness of the interfaces between the layers of the SMs. Due to this imperfectness some neutrons are transmitted through the interface rather than reflected and consequently the reflectivity of the entire multilayer decreases. The possible reasons of the interface roughness is the inherited surface roughness of the substrate and layers deposited earlier, the lateral inhomogeneity of the layer deposition, the inter-diffusion between layers or the formation of nanocrystals. The interface roughness is manifested in the X-ray and neutron specular reflectivity of the multilayer but the correlation of the lateral inhomogeneities of different interfaces and the lateral dimension of these imperfections is hidden from such investigations. Transmission electron-microscopy would require cross section of the layer system the preparation of which can influence the layer structure under investigation. Atomic force microscopy can characterize surface roughness but it can only be applied to the substrate surface, or to the surface of the

uppermost layer. Moreover, it is practically impossible to sample sufficiently large areas of the ready-made stratified structures.

Neutron SMs have been investigated by off-specular scattering in a number of papers. For example, Maruyama *et al*. (2009), studied interfacial roughness correlation and diffuse scattering of Ion Beam Sputtered NiC-Ti SMs, periodic and band-filter like multilayers. They emphasized the suppression off-specular scattering in NiC-Ti as compared to Ni-Ti multilayers and determined the correlation lengths and roughness of the investigated structures using the Distorted Wave Born Approximation (DWBA). However, this work lacks the lucid explanation of the characteristic features of the scattering pattern. The polarized diffuse scattering from polarizing Fe-Si prototype SMs (actually from periodic structures) was studied by Paul *et al.* (2015). The effect of the substrate bias voltage on magnetic and structural correlations as well as stress, grain size and coercivity of the multilayers was investigated on triode-sputtered samples. The diffuse scattering was reported to stem from both structural and magnetic roughness. Samples with internal stress exhibit Bragg-sheets, the presence of which above the saturation field indicates out-of-plane correlation of the structural roughness. Post-preparation He^+ irradiation was applied (Merkel et al., 2011) to Fe/Si SMs. The treatment relaxed the residual tensile stress of the mirror coating from 1.76 to 0.37 GPa but at an expense of the decrease of both the critical angle reflectivity and the polarization efficiency.

The aim of the present work is to disclose the overall character of the imperfectness in Ni/Ti multilayers and, in particular, the effect of the roughness replication during layer deposition.

Experimental neutron and X-ray off-specular scattering was measured on DC-sputtered Ni-Ti multilayers of primary interest in neutron optical elements. The features of the off-specular detector scans are interpreted for normal and reverse-layer-sequence SMs as well as for periodic structures. The large penetration depth of neutrons allows for gaining information about SM structures as thick as several micrometers. The X-ray experiments due to their higher flux and higher resolution allow for an estimate of the out-of-plane interface roughness correlation length. However, the low penetration depth of X-ray limits its use to periodic structures of small total thickness.

2. Theoretical background

Real interfaces of multilayers comprise intrinsic imperfectness. The height of the j-th interface can be described as the sum of an average height z_j and a position-dependent deviation, δz_j. This deviation can be regarded as a random function of zero expectation value. Roughness is defined as the standard deviation of δz_j:

$$\sigma_j^2 = \left\langle \delta \; z_j^2 \right\rangle \qquad (1)$$

The layer surface z_j is defined by the surface of the previous layer and accumulated roughness during the deposition of the j-th layer. The specular reflectivity of the single j-th interface is decreased by the Nevot-Croce (Nevot & Croce, 1980; de Boer 1994) exponential factor

$$r_j = r_j^{(id)} \exp(-k_j k_{j+1} \sigma_j^2) \qquad (2)$$

where $r_j^{(id)}$ is the reflectivity of the ideal plane interface, k_j and k_{j+1} are the plane perpendicular components of the wave vector inside the two layers surrounding the

interface. Due to the change of the reflectivity of the individual interfaces the roughness influences the specular reflectivity of the entire multilayer. The lateral inhomogeneities are the source of the off-specular scattering.

2.1. Resonant diffuse scattering

In case of perfect layer replication, i.e. of out-of-plane translational symmetry of the interfaces the diffuse scattered waves from the individual interfaces add coherently. Consequently, for a periodic system the interference of the diffuse scattered waves is constructive if the following Bragg-like condition is fulfilled:

$$d(\sin\vartheta_{in} + \sin\vartheta_{out}) = n\lambda \qquad (3)$$

where d is the period of the multilayer, θ_{in} and θ_{out} are the incidence and reflection angle, λ is the wavelength and n is an integer (order) number. The enhanced diffuse scattering appearing under these conditions is called Resonant Diffuse Scattering (RDS) (Holy *et al.* ,1993; Holy & Baumbach, 1994, Kaganer *et al,* 1995 and Daillant and Gibaud, 2009, p.257-260).

2.2. Distorted wave Born approximation

The accurate, but less expressive description of diffuse scattering phenomena including RDS is the Distorted Wave Born Approximation (DWBA) (Sinha *et al.*, 1988; Holy *et al.*,1993; Holy & Baumbach, 1994 and Daillant and Gibaud, 2009, p.145-151). In DWBA the lateral inhomogeneities are taken into account as perturbations. The wave function in the unperturbed case of a laterally homogeneous structure (specular scattering) can be calculated using the Parratt recursion formula (Parratt, 1954) or the supermatrix algorithm (Rühm et al, 1999). The diffuse scattered intensity by a rough multilayer in the DWBA is:

$$I^{diff} = C_{\exp}\sum_{j,k=1}^{N}\sum_{\pm}\Delta\rho_j\Delta\rho_k U_j(\pm k_1)U_j(\pm k_2)U_k^*(\pm k_1)U_k^*(\pm k_2)\; Q_{jk}(q_j, q_k) \quad (4)$$

where $C_{\exp}$ is a factor dependent on the experimental setup, $\Delta\rho_j=\rho_j-\rho_{j-1}$ is the scattering length density contrast between the two sides of the j-th interface. Inside each layer the wave function is the sum of an incoming and outgoing plane wave. $U_j(\pm k)$ is the amplitude of the incoming (sign +) and outgoing (sign –) plane wave in the j-th layer, k is the plane-perpendicular component of the incident wave vector.
The $Q_{j,k}(q_j,q_k)$ term is determined by the statistical properties of the lateral inhomogeneities

$$Q_{j,k}(q_j, q_k) = 2\pi A\frac{\exp\left[-(q_j^2\left\langle\delta\, z_j^2\right\rangle + q_k^{*2}\left\langle\delta\, z_k^2\right\rangle)/2\right]}{q_j q_k^*}\int dR_{II}J_0(q_{II}R_{II})R_{II}\left[\exp(q_j q_k^*\left\langle\delta\, z_j(\underline{0})\delta\, z_k(\underline{R}_{II})\right\rangle) - 1\right]$$

(5)

Let σ_j be the interface roughness of j-th interface according to (1). The correlation between laterally sufficiently distant points of the interface vanishes. Let ξ_{II} be the in-plane correlation length determining the length scale of this correlation.
The height-height self- (or auto-) correlation of interface j is described by:

$$\left\langle \delta z_j(0)\delta z_j(R_{II})\right\rangle = \sigma_j^2 \exp[-(R_{II}/\xi_{II})^{2h}] \quad (6)$$

The $0<h<1$ Hurst exponent is related to the fractal dimension d of the interface (d=3-h) (Sinha et al., 1988; Daillant & Gibaud 2009, p65-66). Small values of the Hurst parameter indicate a strongly jagged interface profile, whereas values close to unity indicate a smoothly varying interface.

A layer by layer grown multilayer has an intrinsic correlation between the interface roughness in the lateral and in the vertical directions. This leads to the need for describing the roughness correlation between different interfaces j and k.

The form of the j-th interface depends on the deposition of the layer and the surface of the previous interface, (j-1).

$$\delta z_j(r_{II}) = a_{j-1}(r_{II}) + \int \delta z_{j-1}(R_{II}) b_{j-1}(r_{II} - R_{II}) dR_{II} \quad (7)$$

Here the random function a and the replication function b are statistically independent. Using a replication function of form $b_j(r_{II})=b_j\delta(r_{II})$, with $\delta(r_{II})$ being the Dirac-delta function

$$Q_{jk} = Q_{kk} \prod_{k<i<j} b_i \qquad (j>k) \quad (8)$$

If we assume b_i to exponentially decrease with the layer thickness, we get the widely used expression for the roughness correlations. The length scale of the exponential decay is the out-of-plane correlation length, Λ (Daillant & Gibaud, 2009, p239-240 and p258; Ming *et al.,* 1993):

$$\left\langle z_j(0) z_k(R_{II})\right\rangle = \sigma_j \sigma_k \exp[-(R_{II}/\xi_{II})^{2h}] \exp[-\left|z_j - z_k\right|/\Lambda] \quad (9)$$

There are important differences between the result of the simple kinematical approach (the unperturbated states are plane waves) and that of DWBA. Namely, observable phenomena appear in DWBA due to the enhancement of the wave function in the layer system. These features are the Yoneda (Yoneda, 1963) and the dynamical Bragg-like peaks (Kaganer et al., 1995) at q-values where the angle of incidence or the angle of reflection equal to the critical angle of reflection of the material or Bragg angles of the multilayer.

Due to refraction, the positions of the RDS peaks are shifted as compared to (3). At higher angles the dynamically and kinematically calculated positions of these peaks approach each other. The strength of RDS is influenced by the amplitude of the wave function. If $Q_{j,k}$ differ for the different layers, the RDS peaks are decreased, broadened or – in the absence of out-of-plane correlation – may even disappear.

3. Experimental details

3.1. Samples

Two kinds of samples were used in the present study: periodic multilayers and aperiodic supermirrors with m=3 (normal sequence samples) and m=2.5 (reverse sequence sample). Both structures consist of Ni(11at% Mo)/Ti bilayers. The Ni(Mo)/Ti is the most widely used non-magnetic neutron SM structure. Ni containing more than 8 at% Mo is nonmagnetic at ambient temperature (Vogt and Höhl, 1962). This property of the multilayer is essential. The neutron-optical device has to be non-magnetic to avoid

depolarization of a polarized neutron beam. Ni(Mo)/Ti is as suitable for SM production as Ni/Ti because the scattering length difference between Ni and Ni(Mo) in this concentration range is negligible. The samples were deposited by dc magnetron sputtering (Kovács-Mezei et al., 2008) onto borofloat glass substrates (200×80 mm in size, rms surface roughness of 2-3 Å) at Mirrotron Ltd. (Budapest) by automatic control of the predesigned layer structure. DC sputtering is the most widely used preparation method for large scale neutron SM production.

3.1.1. Periodic multilayer samples

In order to measure the out-of-plane correlation length simple periodic multilayers were prepared for x-ray reflectivity measurements. $\{Ni(Mo)[x]/Ti[y]\}_n$ samples with n=8 and (x,y)= (69, 57) Å, (96, 67) Å and (118, 85) Å were grown by the same method using the same Ni(Mo)/Ti targets. The choice of the number of layers was a compromise of two conflicting conditions. On the one hand a suitably large number of interfaces was needed to study the off-specular scattering. Moreover, it is easier to measure the broadening of a narrower peak (larger repetition number). On the other hand, due to the finite penetration depth of X-rays, large number of layers is disadvantageous. As a compromise, our samples consisted of 8 bilayers. The sample structures are summarized in Table 1.

Table 1

The data of investigated periodic multilayer samples of glass/$[Ti(d_{Ti})/Ni]d_{Ni})]_8$ structure. Λ_{min} is the lower estimate of the out-of-plane correlation length (see Sec. 4.1).

Sample ID	d_{Ni}(Å)	d_{Ti}(Å)	Λ_{min}(Å)
P-A	69	57	1000
P-B	96	67	3500
P-C	118	85	3100

3.1.2. SM samples

Neutron SM structures are conventionally characterized by the (generally non-integer) number m, giving the (wavelength-dependent) critical angle of the structure (θ_{cr}) in units of that of natural nickel, $\theta_{cr(SM)}=m\cdot\theta_{cr(Ni)}$. The investigated SM samples were of m=2.5 and m=3. The layer structures were designed by the Hayter-Mook algorithm (Hayter & Mook, 1989). The SM layer sequence in normal case began with the thinnest layers at the substrate and ended with the thickest. For providing high reflectivity below the Ni critical angle the very last layer was a thick capping Ni layer. The specular reflectivity of a SM is close to 100 % below the critical angle of Ni where a linear decrease begins until $m\cdot\theta_{cr(Ni)}$. In the absence of absorption it would be indifferent whether this is the layer order or a reverse one. In the case of reverse SMs at low incidence angle the neutrons are reflected by thick layers close to the substrate. This long path in the SM material lead to increased absorption and a well is observed in the reflectivity curve of reverse SMs. In our experiments most multilayers were of "normal" sequence, but one SM was produced with the "reverse" layer sequence.

Another parameter of the SMs is the limiting reflectivity just below the critical angle of reflection of the multilayer structure. The interface structure and roughness considerably influences the limiting reflectivity of SMs and consequently their "quality", i.e. usefulness for neutron optical purposes. The limiting reflectivities of the used samples were between 60 and 89%. The SM sample structures are summarized in Table 2.

Table 2
The data of investigated SM samples. The sample ID, the m value, the layer sequence (normal or reverese) and the critical angle reflectivity, R_c. In the case of reverse SMs the R_c values in parentheses correspond to the minimum reflectivity of the dip in the reflectivity curve.

Sample-ID	m	Sequence	R_c
S-1	2.5	normal	0.89
S-2	2.5	reverse	0.86(0.69)
S-3	3.0	normal	0.60
S-4	3.0	normal	0.71
S-5	3.0	normal	0.75
S-6	3.0	normal	0.80
S-7	3.0	normal	0.81
S-8	3.0	normal	0.88
S-9	5.0	reverse	0.4(0.3)
S-10	5.0	normal	0.71

3.2. Instrumentation

X-ray measurements were carried out on a Philips X'Pert MPD diffractometer using Cu X-ray tube (0.15418 nm wavelength) and Goebel mirror for producing quasi parallel beams (0.05 degrees of angular divergence). The beam intensities were recorded with a scintillation point detector equipped with copper foil attenuators to reduce the intensity at angles where necessary. In order to reduce the illuminated area (better resolution, reduced parasitic scattering) a beam knife edge was carefully positioned over the sample surface. The final angular resolution was about 0.01 degree.

Most neutron reflectograms were recorded on the REF constant-wavelength (λ = 4.28 Å) neutron reflectometer at the Budapest Research Reactor. The collimation was provided by two slits (width and height of 1 and 80 mm, respectively) at a distance of 2 m from each other. The scattered neutrons were detected by a 20x20 cm^2 position-sensitive ^3He detector (spatial resolution of 2 mm) at 160 cm distance from the sample. This experimental setup makes the detector-scan a convenient method of measuring diffuse scattering. The neutron reflectivity of m=5 SMs were measured on the GINA reflectometer at λ=4.67 Å (Bottyán et al., 2013) in order to cover the necessary extended angular range.

Multilayers may exhibit lateral inhomogeneities of different length scales i. e. of different correlation lengths. The (typically periodic) waviness on a larger scale affects the scattering curves in a similar way as the beam divergence. The (stochastic) roughness on the microscopic scale leads to an exponential decrease of the interface reflectivity (see eq. (2)). The macroscopic and microscopic regimes are distinguished by the coherence length of the scattering experiment. Consequently, the neutron coherence length is the upper limit of the structural correlation lengths that can be investigated in a given reflectometric

experiment. It is estimated from the Q-vector uncertainty. Using the values of collimation given by the slits and the angular resolution of the detector in the experiments presented here the coherence length in the beam direction varied between 2800 and 18000 Å depending on the angles of incidence and reflection.
The estimated angular uncertainty, $\Delta\varphi$ perpendicular to the collimation direction was ~10 mrad. Therefore the coherence length in the direction perpendicular to the scattering plane is about 25 Å, much shorter than in the parallel direction.

3.3. Reflectometry: Q-regimes of off-specular scattering

For an off-specular scattering study the ideal procedure is to map the available q-space. However, in many cases the experimental conditions only allow to measure the scattered intensity in a restricted region or even only along particular lines in the q-space. The different scans of q-space provide different information about the investigated system (Daillant & Gibaud, 2009, p242-243). The features like Yoneda-peaks, dynamical Bragg-like peaks appear if the incident or exit angle takes some particular values. The lines corresponding to these conditions are almost perpendicular to an ω-scan. In these conditions the dynamical features provide peaks in the experimental curve. To observe RDS peaks providing information on the roughness correlation of various interfaces the suitable geometries are the detector-scans and the $\Delta\theta$–$\Delta 2\theta$ scans. (The latter is when the sample normal and the detector are rotated at angles in a ratio of 1:2, so that the sample normal and the bisector of the incident and detected beams have a constant "offset" angle.) These scans are sketched in the map of q-space in Fig. 1.

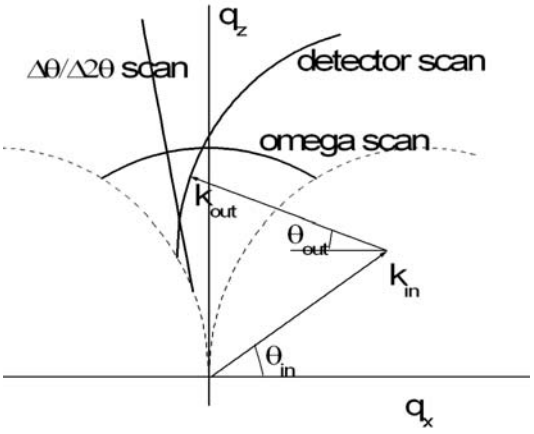

Figure 1
The off-specular detector scans, the $\Delta\theta/\Delta 2\theta$ scans and the ω-scans are indicated as described in the text. The offset angle is the angle between the $\Delta\theta/\Delta 2\theta$ scan line and q_z. The dashed lines represent the border of the non-observable region of the q-space at a given wavelength. For the sake of visibility the angles are grossly increased. The measurable reflectivity range is limited to a few degrees of θ_{in} and θ_{out}.

4. Experimental results and interpretation

4.1. Off-specular X-ray scattering from periodic multilayers

Due to the common deposition process and the common substrate surface quality, similar replication behavior is expected for Ni(Mo)-Ti periodic multilayers and SMs. In order to

get quantitative information about the out-of-plane roughness correlation, model periodic multilayer systems were studied which are much easier to handle theoretically. In the case of a detector scan or $\Delta\theta$–$\Delta 2\theta$ scan the RDS from a periodic system appears in the form of discrete peaks. The relatively small total thickness of these samples makes the X-ray reflectometry applicable. The higher flux and lower background and the consequently higher resolution by x-rays is important in observing the possible broadening of the peaks. The increase of the measured peak widths due to the finite intrinsic angular resolution ($\theta = 0.01°$) of the Philips MPD x-ray diffractometer is negligible.

In Fig. 2 specular and off-specular $\Delta\theta$–$\Delta 2\theta$ scans are displayed for a periodic multilayer sample consisting of 8 bilayers (96 Å Ni and 67 Å Ti). The sharp peaks in the off-specular scans indicate strong correlation of the interface roughness.

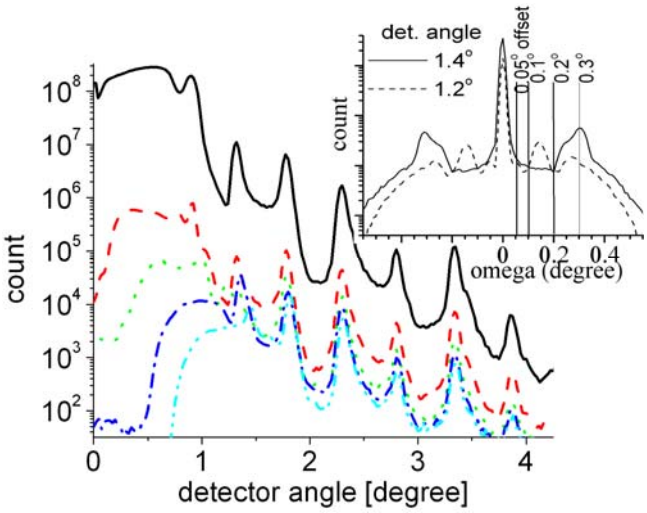

Figure 2

The results of specular and off-specular X-ray $\Delta\theta$–$\Delta 2\theta$ scans (at λ = 1.54 Å) as a function of the detector angle (2θ) for a periodic multilayer sample consisting of 8 bilayers (96 Å Ni and 67 Å Ti) using offsets of 0, 0.05, 0.1, 0.2 and 0.3° from top to bottom, respectively. The inset shows the ω-scan for detector angles 1.2 and 1.4° with the applied offset angles in the main figure. The off-specular scans were recorded outside the specular range (dependent on the resolution).

The specular and off-specular scans of two additional periodic samples (not shown here) are similar and the results of their evaluation are included in Table 3. The widths of the observed peaks were determined by fitting a Gaussian to the measured data points. Table 3 displays the (average) full-widths at half maximum and the standard deviations for each scan. Here the angular unit is the angular distance of the neighboring peaks. The number of peaks taken into account in averaging is displayed for each scan. Peaks of too low intensity (the peak intensity of which was lower than 3 times the background in the corresponding angular range) and peaks close to the dynamical Bragg-like peaks (e.g. peak in scan with 0.1° in Fig. 2) were omitted.

The standard deviation of the peak widths for a $\Delta\theta$–$\Delta 2\theta$ scan with given offset is close to the average peak width difference for the different offsets. The average offset peak widths varied from values smaller to larger than the specular peak width. The specular and off-specular average peak widths were 0.123 and 0.126, 0.146 and 0.144 and 0.142 and 0.141 and the standard deviations were 0.036; 0.01 and 0.015 for sample P-A, P-B

and P-C, respectively. With these values we can assert that no peak broadening was detected within the standard deviation of a single scan.

Table 3
The average peak width and its standard deviation σ (in units of the average peak distance) for the different samples and offsets (in degrees) and the number of the peaks, N of the scan considered in the averaging. "APD" is the average peak distance. The last column "off" contains the average width and its standard deviation for all off-specular peaks considered.

P-A: $[Ni(69Å)/Ti(57Å)]_8$, APD=0.685º

offset	0	0.05	0.1	0.2	0.3	Off
width	0.123	0.126	0.102	0.153	0.128	0.127
σ	0.036	0.023	0.023	0.036	0.018	0.029
N	6	5	4	3	4	16

P-B: $[Ni(96Å)/Ti(67Å)]_8$, APD=0.513º

offset	0	0.05	0.1	0.2	0.3	Off
width	0.146	0.142	0.145	0.145	0.143	0.144
σ	0.008	0.017	0.005	0.009	0.009	0.01
N	6	6	4	5	4	19

P-C: $[Ni(118Å)/Ti(85Å)]_8$, APD=0.412º

offset	0	0.05	0.1	0.2	0.3	off
width	0.142	0.142	0.136	0.145	0.142	0.141
σ	0.009	0.013	0.018	0.019	0.013	0.016
N	8	8	8	7	6	29

In order to quantify the out-of-plane roughness correlation the following simple model was adopted. The correlation of the different interfaces is included in expression (5) of $Q_{j,k}(q_j,q_k)$. Similar to eq. (9) we assume that

$$Q_{j,k}(q_j,q_k) = Q_0(q_j,q_k)\ exp(-\left|z_j - z_k\right|/\Lambda) = Q_0\ \alpha^{|j-k|} \qquad (10)$$

The correlation decays exponentially with the out-of-plane correlation length, Λ. The bilayer thickness of the periodic multilayer is d, and a replication constant $\alpha = exp(-d/\Lambda)$ is introduced.

The RDS peaks are observable at high angles too, where a kinematical approach is sufficient (multiple reflections omitted). If refraction is neglected too; the wave functions may be substituted by plane waves. At a given angle of incidence and reflection the amplitude of the beam traveling through a bilayer accumulates a phase shift φ and is multiplied by a factor β due to the absorption. We wish to know the peak width of RDS. Within a single peak, β and Q_0 can be taken as constants. In this approximation using (10) and omitting the constants not influencing the peak shape, the intensity is:

$$I = \sum_{j,k=1}^{N} \exp[i\varphi(j-k)]\ \alpha^{|k-j|}\ \beta^{j+k} = \sum_{l=0}^{N} 2\beta^2\ \frac{\beta^{2(N-l)}-1}{\beta^2-1} \cos(l\varphi)(\alpha\beta)^l \qquad (11)$$

The change in phase $\varphi = 2\pi\ d(\sin\vartheta_{in} + \sin\vartheta_{out})/\lambda$ gives the main features of the peak shape. Here N=8 is the number of bilayers, d is the thickness of a bilayer.

In this approximation assuming given replication constant α and attenuation coefficients β one gets a constant peak width. The calculated full widths at half maximum are shown in Fig. 3 for an 8-bilayer sample as a function of the replication constant α (see Eq. (10)) for some values of the attenuation coefficient β.

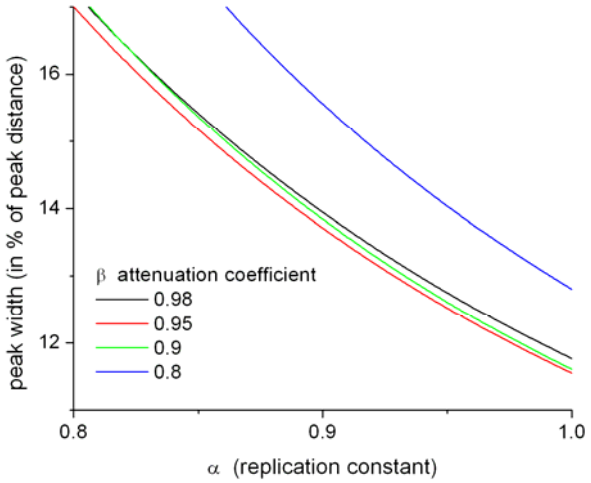

Figure 3
The calculated full width at half maximum as the function of the replication constant according to Eq. (11) for values of the attenuation coefficient indicated in the figure.

There is practically no effect of β on the peak width, if β>0.9. This latter requirement is fulfilled for the peaks displayed in the Table 3. For specular reflection the replication by definition is perfect, α=1.0. Our model gives 12% peak width compared to the peak distance. The average measured width of the specular peaks has the same value for sample P-A but it is higher (14 %) for sample P-B and P-C.
The measured peak widths and their standard deviations for the specular and off-specular $\Delta\theta$–$\Delta 2\theta$ scans should be compared with calculations shown in Figure 3, from which a minimum replication coefficient α_{min} and a minimum out-of-plane correlation length Λ_{min} of 0.88, 0.96 and 0.94 and 1000, 3500 and 3100 Å can be deduced for samples P-A, P-B and P-C, respectively.

4.2. Off-specular neutron scattering from neutron SMs

Detector scans were carried out with monochromatic neutrons on different Ni(Mo)-Ti neutron SM samples, for angles of incidence between the critical angle of Ni and that of the respective SM structure. In Fig. 4 and Fig. 5 the 2D detector pictures (integrated in the slit direction) are displayed for two SM samples.

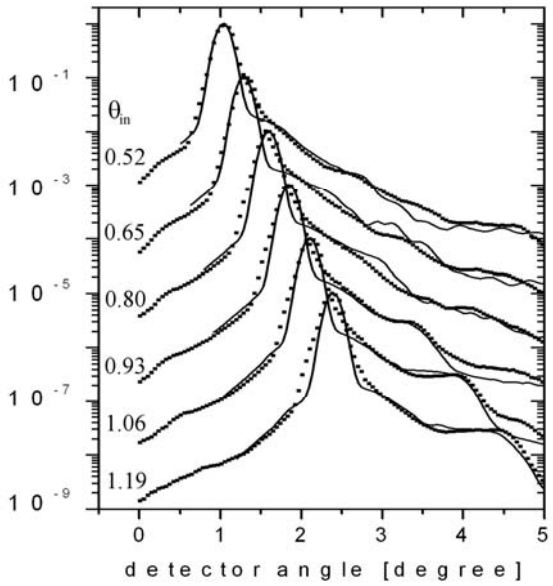

Figure 4
Detector scans of a normal sequence (m=3) SM (S-4 in Table 2) for angles of incidence indicated in the figure at a neutron wavelength of λ=4.28 Å. For the sake of clarity, the scatters for consequtive angles of incidence were shifted in the vertical direction by one order of magnitude. On the high angle side of the specular peak a plateau is observed with a steep declination at about the double of the specular peak angle. DWBA model simulations corresponding to a common interface roughness, in-plane correlation length, out-of-plane correlation length and Hurst exponent of 7, 1200, 4000 Å and 0.5, respectively, are plotted in continuous lines.

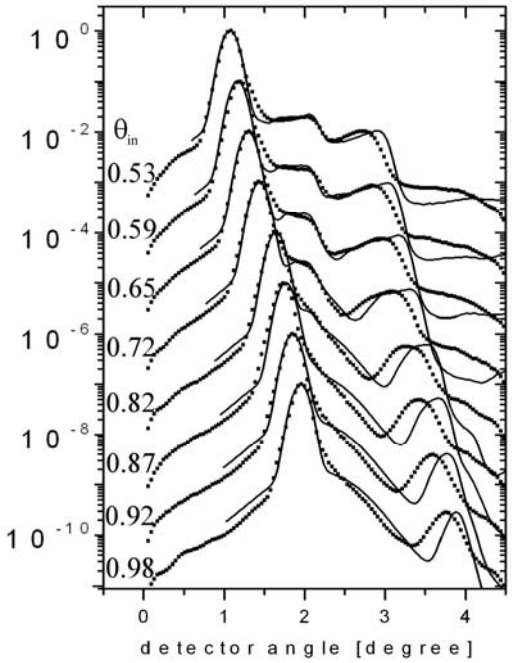

Figure 5

Measured and simulated detector scans of a reverse sequence (m=2.5) SM (S-2 in Table 2) for different angles of incidence indicated in the figure (at a neutron wavelength of λ=4.28 Å). For the sake of clarity, the scatters for consequtive angles of incidence are shifted in the vertical direction by one order of magnitude. On the high angle side of the specular peak a plateau is observed with a steep declination at about the double of the critical angle of the SM independently from the angle of incidence. At roughly the double of the specular peak angle a rather wide peak is observed.
Simulations for a reverse sequence SM (m=2.5) corresponding to a common interface roughness, in-plane and out-of-plane correlation lengths and Hurst exponent of 7, 1200 and 4000 Å and 0.5, respectively, are plotted in continuous lines.

The features of the off-specular scattering were characteristically different for "normal" and "reverse" SMs. For normal SMs a diffuse plateau appears next to the specular peak. The declination point of the curve follows the shift of the angle of incidence and it is located at about the double of the specular angle. For reverse SMs the plateau appears closer to the specular peak. The end of this plateau is constant for a given SM and it is at an angle about twice the critical angle of the SM. It is followed by a wide off-specular peak. This latter peak shifts with the angle of incidence and its position is roughly at double the specular peak angle. Similar features were observed for all used incidence angles in the detector scans for the investigated SMs (of Table 2) not presented in detail.
The investigated structures are rather complex. The normal and reverse sequence SMs with m=2.5, 3 and 5 consist of 320, 550 and 4100 layers, respectively. DWBA model calculations of off-specular neutron reflectivity were carried out for these layer structures by the FitSuite code (Sajti, 2009) with nominal layer thicknesses and theoretical scattering length densities for Ni(Mo) and Ti, respectively. The roughness, the in-plane and out-of-plane correlation lengths as well as the Hurst parameter were assumed to be equal for all interfaces in the calculation. The correlation of the interfaces was considered exponential, according to (9).
The minimum deviation between experiment and simulation was achieved for both SM structures with σ=7Å, h=0.5, ξ_{II} =1200 Å and Λ=4000 Å. However, these parameters can not be regarded as fit results and there is a range for the parameters (Λ between 2800 Å and infinity, other correlation parameters about ±15 %), within which no significant difference is seen in the calculated curves.
The results of calculations are plotted in Fig. 4 for m=3 normal SM for various angles of incidence. Similarly, in Fig. 5 the results for m=2.5 reverse SM is shown. Note, a perfect collimation is assumed in the calculation in the plane perpendicular to the plane of reflection, while the experiment uses a slit geometry. The finite angular resolution was taken into account by numerical convolution of the calculated ideal detector scans with the measured direct beam shape. In the detector scan calculation the specular to off-specular intensity ratio is chosen by the user.
Our DWBA calculation correctly reproduces all angular features of the scans, such as plateau edges, peak positions and widths. The minor differences between experiment and model calculations may stem from the incomplete account for the slit geometry, and the validity of the assumptions (Dirac-delta like replication function of amplitude exponentially decreasing with layer thickness) leading to equation (9) and the uniform roughness of all interfaces. The present rudimentary model does not account for the systematic shift of RDS II peaks in reverse SM. Attempts were made to refine the presented model to account for possible systematic variation of the interface roughness of the consequtive layers. Due to the different diffusion coefficients of Ti in Ni and Ni in Ti

and different surface mobility of the deposited Ni and Ti atoms Ni/Ti and Ti/Ni interfaces may have interdiffused layers of different thickness. Layer growth models indicate thickness-dependent roughness (Karunasiri *et al*., 1989; Drotar *et al.*, 2000) and the surface of the previous layer also influences the roughness leading to an increased (cumulative) roughness of the multilayer (hivatkozás?). Therefore simulations were performed with asymmetric, monotonously increasing and monotonously decreasing Ni/Ti and Ti/Ni roughnesses (of different functional dependence of the layer number). Neither the asymmetric, nor the increasing roughness provided the right *direction* of the shift of the measured RDS II peaks. The only model with strongly decreasing roughness (20Å at the substrate and 4Å at the topmost layer) may account for the variation of the RDS II peak positions. However, in view of the evolution of roughness in multilayer growth (Spiller et al., 1993), such model seems rather unrealistic. In the above attempts, the out-of-plane correlation length was assumed constant. A layer-thickness-dependent out-of-plane correlation may account for larger observed shifts, but such assumption would require confirmation by further (transmission electron)microscopic studies.

The DWBA calculation correctly describes the off-specular scattering processes, but it does not give a physical insight into the differences between the normal and reverse SM scatters. Such features of the off-specular scattering from neutron SMs can be interpreted as the consequence of RDS from a multilayer with slowly varying period using the following simple kinematical considerations.

First let us consider the case of a periodic multilayer investigated with monochromatic neutrons. RDS is observable if condition (3) is fulfilled and there exists a certain correlation of the interface roughness. For $n=1,2,...$ we speak about the first, second, etc. order RDS (RDS-I, RDS-II, …). Let the Bragg angle of the structure be θ_{Br}. In the kinematical approach RDS I and II are observed at detector angles $2\theta_{Br}$ and $4\theta_{Br}$, respectively. In reality, these angles are somewhat modified by refraction, so that the peak positions of RDS-I and RDS-II are only roughly independent of the angle of incidence θ_{in}. If $\theta_{in} < \theta_{Br}$, the RDS-I peak appears at an exit angle $\theta_{out}=(2\theta_{Br}-\theta_{in})>\theta_{Br}$. Similarly, for $\theta_{Br} < \theta_{in}$, the RDS-I peak appears at $\theta_{out} < \theta_{Br}$.
The case of aperiodic SMs is more complex. Instead of the discrete RDS peaks for aperiodic structures wide plateaus are observed. In order that an RDS peak to appear at a certain angle, roughness replication needs to be present in those layers for which condition (3) is fulfilled. The corresponding layers also have to be illuminated and the off-specularly scattered beam has to pass through all overlayers above the corresponding layer. A more precise formulation of this condition is that the wave functions in equation (4) penetrate the corresponding layers of the SM. This only occurs to a depth until the layers which fulfill the Bragg condition for the actual angle of incidence. Due to the opposite layer sequences we deal separately with the normal and reverse SMs below.

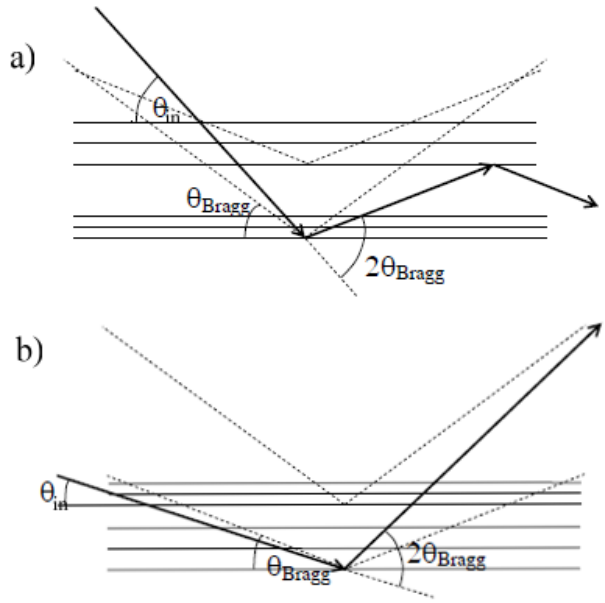

Figure 6
Illustration of the appearance and blocking of RDS-I in case of a) normal and b) reverse SMS, respectively. The parts consisting of thinner and of thicker bilayers of normal and reverse SMs. The dashed lines correspond to the angles of the specular Bragg reflection. The incident beam (at angle θ_{in}) is scattered at an angle $2\theta_{Bragg}$, corresponding to the bilayer at the position of scattering event.
In normal SMs (a) there is an upper part of SM in Bragg position (or if the angle is smaller than θ_{Ni}, there is the thick capping layer) scattering back the RDS-I reflection.
In reverse SM – assuming an exit angle higher than the critical angle of the SM ($m\cdot\theta_{Ni}$) the scattered neutrons penetrate the overlayers.

In normal SMs the upper illuminated layers are thicker than the ones corresponding to the Bragg condition at θ_{in}, and their Bragg angles are $\theta_{Ni}<\theta_{Br}<\theta_{in}$. In the case of RDS-I the exit angle θ_{out} is smaller than the angle of incidence θ_{in} (because $\theta_{Br}<\theta_{in}$, similarly to the periodic case). Above the layers having Bragg angle θ_{Br} the layer structure is a SM of critical angle θ_{Br}, which is not transparent for the RDS-I scattered neutrons ($\theta_{out}<\theta_{Br}$). Consequently RDS-I is not observable. This blocking of RDS-I in case of normal SM is illustrated also in Fig. 6 a).
In the RDS-II case the exit angle is much higher and the overlayers are transparent to it. The scattering angle of RDS-II is four times the Bragg angle of the illuminated layers. Consequently, RDS-II is observable in the angular range between $4\theta_{Ni}$ and $4\theta_{in}$. In Fig. 4 there is no trace of the RDS-I plateau and the end of RDS-II plateau is clearly observable at about $4\theta_{in}$. The end of the RDS-II plateau is at slightly lower angle than the double of the specular peak. The reason can be that the wavefunction does not abruptly decay at the corresponding layer but it begins decaying already at several layers above.
In the reverse SMs the layers of Bragg angles $\theta_{in}<\theta_{Br}<m\theta_{Ni}$ are illuminated. The RDS-I has larger exit angle than the Bragg angle of corresponding layers. The overlayers in this case constitute a band-filter which is not transparent in the angular range between θ_{in} and $m\cdot\theta_{Ni}$. If $\theta_{out}>m\theta_{Ni}$, the scattered neutrons pass through the overlayers and RDS-I appears. Consequently, the Bragg angles θ_{Br} of the layers contributing to the observable RDS the $0.5\cdot(\theta_{in}+m\cdot\theta_{Ni})<\theta_{Br}<m\cdot\theta_{Ni}$. The RDS-I appears between $\theta_{in}+m\cdot\theta_{Ni}$ and $2m\cdot\theta_{Ni}$. For the detector scans where the specular peak does not overlap, the constant breakdown

edge at $2m \cdot \theta_{Ni}$ is clearly seen in Fig. 5. The appearance of RDS-I in case of reverse SM is illustrated in Fig. 6 b).

For the RDS-II there is no simple blocking condition. One can expect RDS-II plateau to appear for detector angles between $4\theta_{in}$ and $4m \cdot \theta_{Ni}$. The increasing edges of observed peaks (Fig. 5) correspond approximately to the lower limit of the plateau, but after the edge there is no plateau until $4m \cdot \theta_{Ni}$ but only a peak. Our simple theoretical considerations can only explain where no RDS can be expected, but fails in forecasting the end of RDS-II plateau in the reverse case. DWBA calculation correctly describes the scattering but the numerical calculations hide the reasons for the characteristic features of the scattering.

Note, that the experimental results do not confirm the simple assumption that the diffuse scattering is smaller for SMs of "better quality". Indeed, intuitively, higher off-specular scattered intensity is assumed from an SM of the same nominal structure but of smaller specular reflectivity. In Fig. 7 specular reflectivity curves and the corresponding off-specular scatters are compared for four normal sequence $m = 3$ supermirrors of critical angle reflectivity of 0.60, 0.71, 0.8 and 0.88, sample-ID S-3, S-4, S-6 and S-8, respectively. As it is apparent from panel *b*), that no direct relation exists between the off-specular (RDS-II) intensity and the critical angle reflectivity. On the one hand, specular reflectivity is principally modified by the thickness deviations from the ideal layer thickness sequence (Hayter & Mook, 1989) even in case of zero interface roughness. On the other hand, interface roughness in an otherwise ideal layer sequence SM affects the specular reflectivity similarly (Veres & Cser, 2015)

Moreover, the off-specular intensity is considerably determined by the out-of-plane correlation of the interface roughness, a feature not present in case of specular scattering.

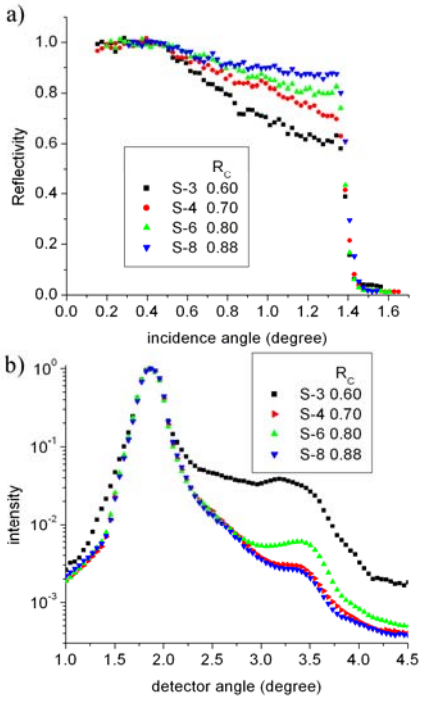

Figure 7

a) The specular reflectivity curves of m=3 SMs of different critical angle reflectivities. b) The off-specular scattering of these SMs at an angle of incidence of 0.95°. No direct correlation between the intensity of off-specular scattering and the critical reflectivity of the SMs can be inferred form the figure.

Taking into account the uncertainties of the calculations, the value of 4000 Å of out-of-plane correlation lengths used in the simulation of detector-scans for SMs is in acceptable agreement with the lower estimation of a few thousand Ångstoms deduced for periodic multilayer samples.
Finally, taking into account that the simple theoretical considerations explaining the experimental results are based on the presence of roughness replication and that the numerical results are in accordance with the experimental observations only if the roughness replication assumption is valid. As a consequence the roughness replication in SMs and periodic multilayers is proven.

5. Conclusions

The interface roughness and its evolution within the layer sequence of various multilayers was investigated by means of off-specular X-ray and neutron reflectometry. Experimental evidence is given for long range roughness replication in the investigated periodic multilayers and aperiodic supermirror structures by observation of resonant diffuse scatter peaks and plateaus. For DC-sputtered Ni(Mo)-Ti multilayers a lower estimate is deduced for the out-of-plane correlation length based on the absence of broadening of the resonant diffuse X-ray peaks. The first order of RDS is missing in the neutron off-specular scatter of normal but is present in reverse layer sequence supermirrors. The different character of the diffuse neutron scattering from normal and reverse sequence SMs is explained using simple theoretical considerations and confirmed by numerical calculation by the Distorted Wave Born Approximation. A fair agreement of experiment and simulation was found for a common interface roughness, depth-independent in-plane and out.of-plane correlation lengths and Hurst parameter of σ=7Å, ξ_{II} =1200 Å and Λ_{out}=4000 Å and h=0.5. No correlation was observed between the technically vital critical angle reflectivity and the shape of the roughness-mediated off-specular neutron scattering of six different normal sequence supermirrors. Further studies of roughness correlation in Ni-Ti multilayers are in progress.

Acknowledgements

Preparation of the samples by Mirrotron Ltd. is gratefully acknowledged. The work of one of the authors, Sz. Bálint was supported by the János Bolyai Research Scholarship of the Hungarian Academy of Sciences. The authors are grateful to László Bottyán for helpful discussions and his critical reading of the manuscript.

References

de Boer, D. K. G. (1994) *Phys. Rev. B.* **49,** 5817-5820.
L. Bottyán, D.G. Merkel, B. Nagy, J. Füzi, Sz. Sajti, L. Deák, G. Endrőczi, A.V. Petrenko, J. Major (2013) *Rev. Sci. Instrum.* **84,** 015112 1-8.

Daillant, J. & Gibaud, A. (2009) Editors. *X-ray and Neutron Reflectivity*. Berlin Heidelberg: Springer.
Drotar, J. T., Zhao, Y.-P., Lu, T.-M. and Wang, G.-C. (2000) *Phys. rev. B.* **62,** 2118-2125.
Hayter, J. B., Mook., H. A. (1989) *J. Appl. Cryst.* **22,** 35-41.
Holy, V., Kubena, J., Ohlídal, I., Lischka, K., & Plotz, W. (1993) *Phys. Rev. B* **47,** 15896-15903.
Holy, V. & Baumbach, T. (1994) *Phys. Rev. B*. **49,** 10668-10676.
Kaganer, V. M., Stepanov, S. A. & Köhler, R. (1995) *Phys. Rev. B* **52,** 16369-16372.
Karunasiri, R. P. U., Bruinsma, R. &Rudnick, J. (1989) *Phys. rev. Letters* **62** (1989) 788-791.
Kovács-Mezei, R., Krist, T. & Révay, Zs. (2008) *Nucl. Instr. Methods A* **586,** (2008) 51-54.
Maruyama, R., Yamazaki, D., Ebisawa, T. & Soyama, K. (2009) *J. Appl. Phys*. **105,** 083527 1-8.
Merkel D.G., Horváth Z.E., Szőcs D.E., Kovács-Mezei R., Kertész G.Gy., Bottyán L. (2011) *Physica B: Condensed Matter* **406,** 3238-3242
Mezei, F. (1976) *Commun. Phys.* **1,** 81-85.
Mezei, F. & Dagleish, P. A. (1977) *Commun. Phys.* **2,** 41-43.
Ming, Z. H., Krol, A., Soo, Y. L., Kao, Y. H., Park, J. S. & Wang, K. L. (1993) *Phys. Rev. B.* **47,** 16373-16381.
Nevot, L. & Croce, P. (1980) *Rev. Phys. Appl.* **15,** 761-779.
Parratt, L. G. (1954) *Phys. Rev.* **95**, 359-369.
Paul, A., Teichert, A., Krist, Th. & Steitz, R. (2015) *J. Appl. Cryst.* **48,** 1023-1033.
Rühm, A., Toperverg, B. P. & Dosch (1999) *Phys. Rev. B.* **60,** 16073-16077.
Sajti, Sz. (2009) FitSuite (http://arxiv.org/abs/0907.2805v1) is freely downloadable from its homepage http://www.fs.kfki.hu
Sinha, S. K., Sirota, E. B., Garoff, S. & Stanley, H. B. (1988) *Phys. Rev. B.* **38**, 2297-2311.
Spiller, E., Stearns, D. & Krumrey, M. (1993) *J. Appl. Phys.* **74,** 107-118.
Veres, T. & Cser, L. (2015) *Pollack Periodica* **10,** 71-80.
Vogt, E. & Höhl, M. (1962) in Vol. **9** of Landolt-Borstein ed. Hellwege, K.H. & Hellwege, A.M. p1-55
Yoneda, Y. (1963) *Phys. Rev.* **131**, 2010-2013.